Zahn, R., Comas, M.C., and Klaus, A. (Eds.), 1999
Proceedings of the Ocean Drilling Program, Scientific Results, Vol. 161

4. PLIOCENE–PLEISTOCENE SEDIMENTARY FACIES AT SITE 976: DEPOSITIONAL HISTORY IN THE NORTHWESTERN ALBORAN SEA[1]

B. Alonso,[2] G. Ercilla,[2] F. Martínez-Ruíz,[3] J. Baraza,[2] and A. Galimont[2]

ABSTRACT

The Pliocene and Pleistocene deposits recovered at Site 976 from the northwestern Alboran Sea at the Málaga base-of-slope include five main sedimentary facies: hemipelagic, turbidite, homogeneous gravity-flow, contourite, and debris-flow facies. The thickness and vertical distribution of these facies into lithostratigraphic Units I, II, and III show that the turbidites and hemipelagic facies are the dominant associations. The Pliocene and Pleistocene depositional history has been divided into three sedimentary stages: Stage I of early Pliocene age, in which hemipelagic and low-energy turbidites were the dominant processes; Stage II of early Pleistocene/late Pliocene age, in which the dominant processes were the turbidity currents interrupted by short episodes of other gravity flows (debris-flows and homogeneous gravity-flow facies) and bottom currents; and Stage III of Pleistocene age, in which both hemipelagic and low-energy gravity-flow processes occurred. The sedimentation during these three stages was controlled mainly by sea-level changes and also by the sediment supply that caused rapid terrigenous sedimentation variations from a proximal source represented by the Fuengirola Canyon.

INTRODUCTION

Site 976 is located in the northwestern Alboran Basin at a water depth of 1108 m on the southern part of Málaga margin, 8 km northeast of Deep Sea Drilling Project Site 121 (Shipboard Scientific Party, 1996) (Fig. 1). Site 976 was drilled on a basement high and comprises sediments from the middle Miocene to Pleistocene, part of which were also recovered at Site 121 (Shipboard Scientific Party, 1973). Although the priority at Site 976 was to drill at least 200 m into the predicted metamorphic basement, the recovery of sediments overlying the basement also provides an assessment of the Pliocene and Pleistocene history of the northwestern Alboran margin. Four lithostratigraphic Units (I–IV) were identified in the 669 m of Pleistocene–Miocene deposits at Site 976 (Fig. 2; Shipboard Scientific Party, 1996). In this investigation, we studied sediments from Hole 976B (1108 mbsl) of Unit III to Unit I, ranging in age from Pliocene to Pleistocene. Unit I (0–362.1 meters below seafloor [mbsf], Hole 976B) is of Pleistocene–late Pliocene age; Unit II (362.1–518.3 mbsf, Hole 976B) is late Pliocene in age; and Unit III (518.3–660.2 mbsf, Hole 976B) is early Pliocene–Miocene. This study presents sedimentological and bulk-mineralogical analyses to (1) establish the sedimentary facies at Site 976; (2) determine the facies associations and sediment supply within the vertical stratigraphic successions; (3) discuss the timing of initiation of turbidity-current sedimentation; and (4) establish the depositional history.

GEOLOGICAL SETTING AND BACKGROUND

The Alboran Sea is a narrow (~150 km wide and 350 km long) extensional basin formed during the early Miocene (Comas et al., 1992; Watts et al., 1993). Several geodynamic hypotheses have been proposed to explain the genesis of the Alboran Basin and the processes responsible for the formation of such a basin at sites of continental collision (Dillon et al., 1980; Dewey et al., 1989). A complex post-Tortonian tectonism modified the stratal architecture of the Miocene basins and margins. The Quaternary sedimentary evolution has been controlled mainly by the interplay of tectonics, sea-level, and climate changes, and a complex ocean circulation (Alonso and Maldonado, 1992; Ercilla et al., 1992; Ercilla and Alonso, 1996). In the area of the northwestern Alboran Sea where Site 976 is located, the slope and base-of-slope are eroded by canyons and gullies and deformed by collapse structures, growth faults, and slumps. Physiographic features in the specific area of the present Málaga margin include (Fig. 1) a relatively narrow shelf (11 km) with the shelf-break at 115 m water depth, a slope of 10 km and gradients of ~2.65°, and a relatively broad base-of-slope (16 km) with a gentler gradient (0.4°; Ercilla et al., 1992, 1994). Four submarine canyons indent the slope of the northwestern Alboran Sea. They are, from east to west, the Fuengirola, Torre Nueva, Baños, and Guadiaro canyons (Fig. 1). These canyons are short, and only the Fuengirola and Torre Nueva reach the base-of-slope (Ercilla et al., 1992).

Multichannel seismic-reflection profiles across Site 976 show a structural high with the top of the acoustic basement at depths ranging from 2 to 2.4 s (two-way traveltime; Shipboard Scientific Party, 1996). Recovery of the Tortonian sequence and the Messinian erosional unconformity (laterally equivalent to the seismic M reflector; Maldonado et al., 1992) are essential to document both the transition from open-marine to restricted conditions and open-marine conditions following the Messinian flooding (Fig. 3). Above the M reflector the Pliocene–Quaternary sediments correspond to the seismic unit I defined by Jurado and Comas (1992). The lower part of the Pliocene deposits has a transparent acoustic character, although locally parallel or divergent reflections alternating with more transparent zones can also be identified (Fig. 3). The upper seismic unit I (Pliocene–Holocene) is characterized by parallel reflectors with a strong acoustic character and variable continuity (Fig. 3). From high-resolution seismic profiles, a detailed picture of the sedimentary architecture of the Pliocene–Quaternary deposits, which are the focus of this paper, was determined by Ercilla et al. (1994) and Ercilla and Alonso (1996) (Fig. 3). The lower Pliocene seismic unit is defined by transparent facies and some discontinuous stratified facies. The upper Pliocene seismic unit is composed of a variety of seismic facies, hemipelagic/

[1]Zahn, R., Comas, M.C., and Klaus, A. (Eds.), 1999. *Proc. ODP, Sci. Results*, 161: College Station, TX (Ocean Drilling Program).
[2]CSIC, Instituto de Ciencias del Mar, Paseo Joan de Borbó s/n, 08039 Barcelona, Spain. Alonso: belen@icm.csic.es
[3]CSIC, Instituto Andaluz de Ciencias de la Tierra, CSIC y Universidad de Granada, Campus Fuerteventura, 18071 Granada, Spain.

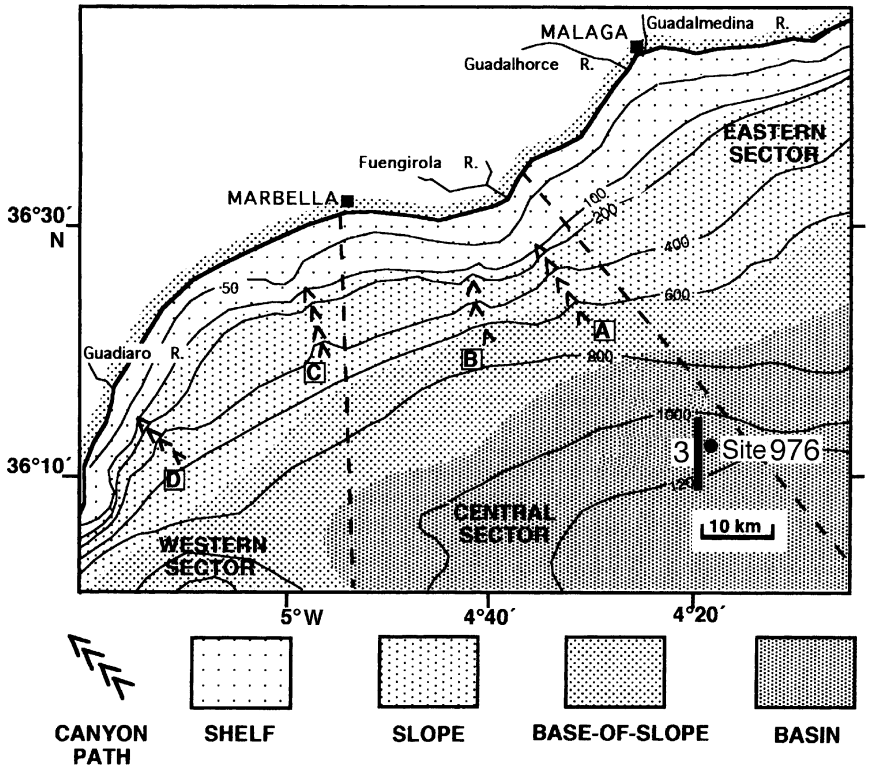

Figure 1. Physiographic provinces of the northwestern Alboran Sea (Málaga margin) showing the canyons' pathways (A–D) and the location of Site 976. Note the proximity of the Site 976 location to the Fuengirola Canyon. Contours are in meters. A = Fuengirola Canyon; B = Torre Nueva Canyon; C = Baños Canyon; D = Guadiaro Canyon; R = river. Discontinuous lines refer to boundaries between geographic sectors. Thick short line labeled with number 3 refers to seismic profile shown in Figure 3. From Ercilla et al. (1994).

gravitative facies intercalated with lobe-wedge facies and channel-levee facies. The Quaternary seismic unit is made up of sediments on the outer shelf that continues seaward into slope and base-of-slope lowstand deposits defined by Ercilla et al. (1994; Fig. 3).

METHODS

Sediment texture analyses of 102 samples were performed using a settling tube for the coarse-grained fraction (>50 mm) and a Sedigraph 5000 D for the fine-grained fraction (<50 mm; Giró and Maldonado, 1985). Textural statistical parameters (mean, standard deviation, skewness, and kurtosis) were calculated using moment measurements on sample populations containing 1/2 ϕ-interval classes in all fractions (Friedman and Sanders, 1978; Swan et al., 1979; Forrest and Clark, 1989). The standard deviation adopted for the classification of sediments into sorting classes (Friedman and Sanders, 1978; Swan et al., 1979; Alonso and Maldonado, 1990; Ercilla et al., 1994) are the following: 0.50 ϕ–0.80 ϕ for well-sorted sediments; 0.80 ϕ–1.40 ϕ for moderately sorted sediments; 1.40 ϕ–2.00 ϕ for poorly sorted sediments; and 2.00 ϕ–2.60 ϕ for very poorly sorted sediments. Sand fraction components were identified using a binocular microscope and by point counting ~400 grains per sample. The components identified and counted are the following: biogenic components (pelagic foraminifers, benthic foraminifers, pteropods, siliceous biogenic components), light minerals (quartz, mica, feldspar, and others), heavy minerals, rock fragments, and neoformation minerals (pyrite and pyritized burrows and tests). The carbonate content of the samples were determined using a Bernard calcimeter, according to the method described by Vatan (1967). Standardless methods of quantitative X-ray analysis were used for the quantitative definition mineral phases. The methodology used for the bulk-mineralogy analyses is explained in Martínez-Ruíz et al. (Chap. 2, this volume).

RESULTS

Major Sedimentary Facies

Pliocene and Pleistocene sediments from Site 976 consist mainly of hemipelagic and turbidite facies, according to the terminology of Stow and Piper (1984). Other sedimentary facies present at Site 976, although less common, include homogeneous gravity-flow, contourite, and debris-flow facies. The distinction of hemipelagic and turbidite material in mud-rich, deep-sea sediment and sedimentary rocks seems to be a common problem (Krenmayr, 1996). In addition, the problem becomes more complicated with the recognition of sediments deposited or reworked by bottom currents (Stow and Faugères, 1993). The sand-fraction composition, sorting, and vertical distribution, but especially grain size, are important criteria for recognizing genetically different deep-sea sediments; all were analyzed in this study (see also Rupke and Stanley, 1974; Hesse and Butt, 1976; Alonso and Maldonado, 1990; Porebski et al., 1991).

A summary of sedimentological data and the relative percentages of the major crystalline components (phyllosilicate, quartz, feldspar, calcite, and dolomite) corresponding to the bulk-mineralogical analysis for Hole 976B is given in Table 1 and in Table 3 (on CD-ROM, this volume). The correlation matrix of sedimentological and mineralogical parameters is shown in Table 2.

Hemipelagic Facies

The hemipelagic term applied in this paper follows the description of Bates and Jackson (1987): "...deep-sea sediments containing a small amount of terrigenous material as well as remains of pelagic organisms..." and also the definition of Stow (1994), who applies this term in the sense of "terrigenous elements (clay, quartz, feldspar, volcanic dust, and other minerals) with a high proportion of silt-sized grains can form a significant part of the settling material and hence of the resulting hemipelagic deposit."

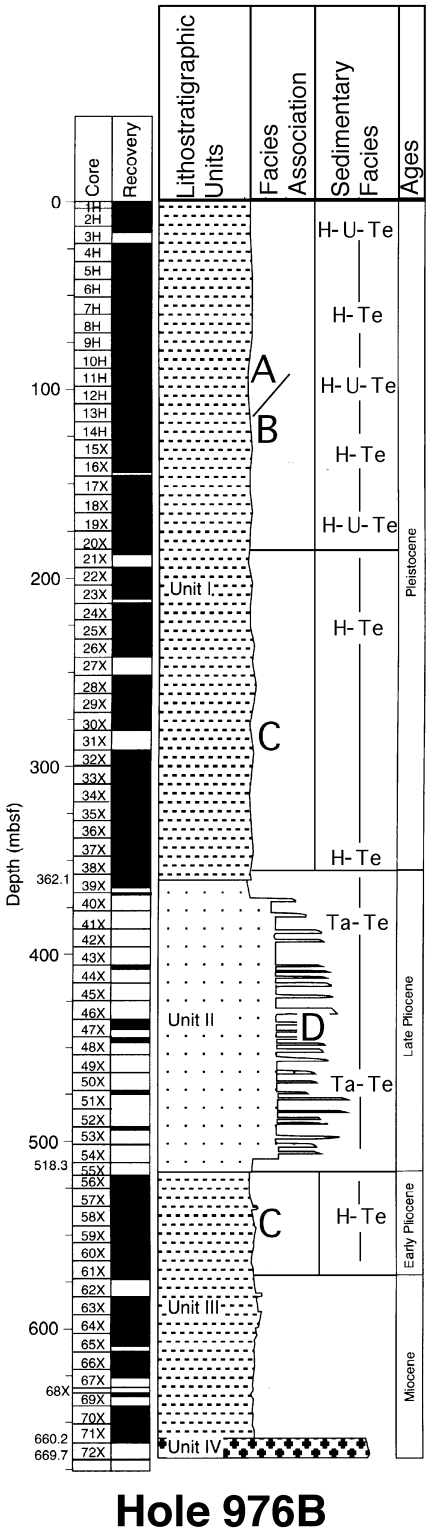

Figure 2. Lithostratigraphic units defined at Hole 976B showing the dominant facies associations (A–D) and the sedimentary facies defined in this work: A = turbidite mud-homogeneous gravity flows, hemipelagic mud (Te–U–H); B = turbidite mud-homogeneous gravity flows (Te–U); C = turbidite mud-hemipelagic mud (Te–H); D = turbidite sand-silt-mud (Ta–Te). Black area refers to the sediment recovery.

Sedimentological Characteristics

The hemipelagic facies is comprised of poorly and very poorly sorted muds (1.5 ϕ–2.6 ϕ) with a mean grain size of 8.0 ϕ–9.1 ϕ and a bimodal grain-size distribution (Fig. 4). Two sedimentary facies types are recognized in this group: H1 and H2, the main differences being the carbonate content and sand-fraction composition. The H1 type is hemipelagic mud a with low carbonate content (<20%). The sand fraction (<9%) is formed mainly of biogenous components (66%–100%), which are represented by radiolarians, diatoms, and silicoflagellates. The H2 type is hemipelagic mud with a relatively high carbonate content (≤44%). The sand fraction (≤9%) is composed mainly of well and moderately preserved planktonic foraminifers (≤90%). In both types, H1 and H2, the hemipelagic facies are structurally homogeneous deposits and bioturbation is the only type of sedimentary structure observed. The color of the hemipelagic sediments varies from moderate olive brown (5Y4/4) to grayish olive (10Y4/2), grayish olive gray (5Y4/1), dark greenish gray (5GY4/1), olive gray (5Y4/1), and light olive gray (5Y5/2).

Bulk-Mineralogical Characteristics

The hemipelagic sedimentary facies is also characterized by significant differences in the bulk mineralogy (Fig. 5; Table 1). It shows a high abundance of phyllosilicates (36%–59%), with a low abundance of quartz (12%–23%), the highest values of calcite (18%–48%), and a very low dolomite (<5%–10%) content. Except for the calcite percentages, the percentages of these mineralogical components are similar in both hemipelagic sediment types, H1 and H2. The minimum values of calcite correspond to the H1 type mud, with a low carbonate content (<20%), and the maximum values of calcite (average of 31%) belong to the H2 type mud with a high carbonate content. This suggests that calcite and carbonate content are correlated. This fact is also supported by the high correlation coefficient (0.65) between the two parameters (Fig. 5; Table 2).

Turbidite Facies

Sedimentological Characteristics

The sedimentary facies of this group is characterized by three different types of texture: sand, silt, and clay. We identified the different divisions of the Bouma sequence: Ta, Tb, Tc, Td, and Te (Figs. 6, 7). The sand fraction of all the divisions is composed mainly of terrigenous components (43%–100%), which, in order of abundance, are light minerals (average of 43%), of which quartz is predominant (average of 30%), mica (average of 3%), and rock fragments (average of 0.5%). In some samples included in the Ta division (897B-52X-1, 28–30 cm; 53X-1, 9–11 cm; 53X-1, 15–17 cm; 53X-2, 6–8 cm; 54X-1, 27–29 cm), quartz is the most abundant component (70%–85%). The color of the turbidite sediments is related in general to the texture. Thus, the turbidite muddy sediments are mainly dark greenish gray (5GY4/1) and, in minor proportions, are olive gray (5Y4/1), grayish olive gray (5G53/2), and grayish olive green (5GY3/2). The silty sediments are generally darker (medium dark gray, N4), as are the sandy sediments (dark gray, N3; medium dark gray, N4; olive gray, 5Y4/1). The Ta division corresponds to moderately well-sorted (0.8 ϕ–1.4 ϕ) and moderately sorted (1.1 ϕ–1.4 ϕ) fine sands, with a mean grain size of 2 ϕ. The carbonate content is low (15%–16%). Some layers appear as medium-grained sands with a normal vertical gradation. The Tb division corresponds to moderately sorted (0.9 ϕ–1.0 ϕ) silty sand (Fig. 6A). The Tb division has modes between 1 ϕ and 3 ϕ, with tails toward the fine-grained fractions (Fig. 4), and a mean grain size between 1.1 ϕ and 1.8 ϕ. The carbonate content ranges from 13% to 17%. The Tc division corresponds to very poorly

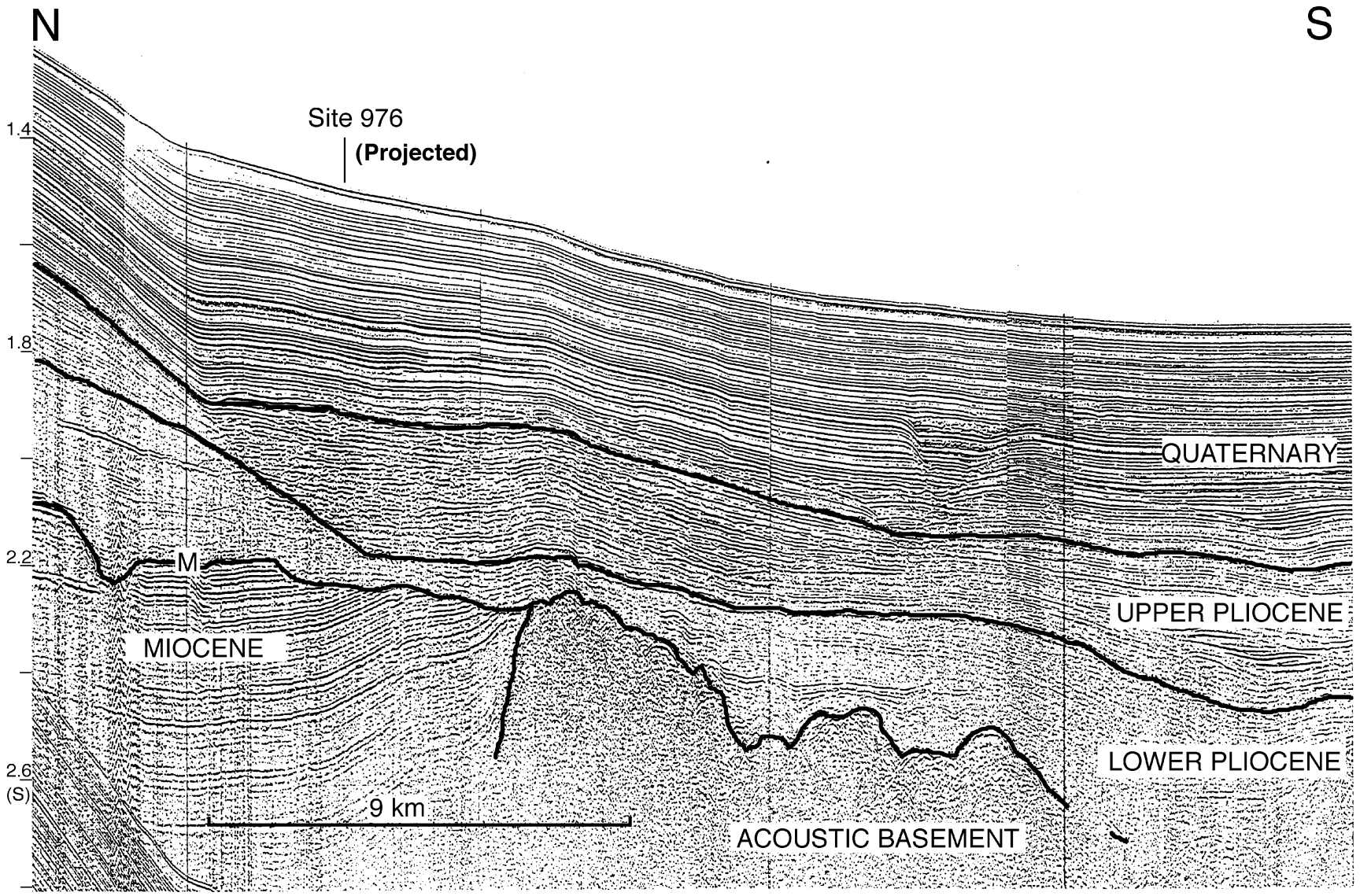

Figure 3. High-resolution seismic profile (air gun) showing the seismic units from Miocene to Quaternary, as well as the projected location of Site 976. Note the channel-levee complexes developed within the upper Pliocene seismic unit. Location is indicated in Figure 1.

Table 1. Textural, compositional, and bulk mineralogical data from Hole 976B.

Sedimentary Facies	Sedimentological Parameters										Mineralogical Parameters				
	Biogenous (%)	Terrigenous (%)	$CaCO_3$ (%)	Sand (%)	Silt (%)	Clay (%)	Mean (phi)	Sorting (phi)	Skewness (phi)	Kurtosis (phi)	Phyllosilicate (%)	Quartz (%)	Feldspar (%)	Calcite (%)	Dolomite (%)
Hemipelagite															
H1	66-100	0-34	13-20	0.9-2.0	25-40	59-74	8.5-9.1	1.5-1.8	0.1-0.2	2.2-2.3	37-59	17-23		18-32	<5-8
H2	61-90	10-40	20-44	1.5-8.9	22-37	55-77	8.0-8.9	1.7-2.6	0.9-0.1	2.1-4.8	36-51	12-21		24-48	<5-10
Turbidite															
Ta	0.1-0.9	99-100	15-16	71-72	27-28	0.1-0.5	1.2-1.5	0.8-1.4	0.7-1.2	1.8-2.7	10-14	46-63	5-6	18-24	5-21
Tb	0.3-0.9	97-100	13-17	50-63	36-49	0.1-0.4	1.1-1.8	0.9-1.0	1.1-1.6	2.2-3.5	11-14	46-51	<5	18-21	16-22
Tc	0.5-0.9	94-100	14-22	45-61	25-30	11-18	4.4-5.0	2.6-3.3	0.6-0.9	2.3-2.8	5 -15	28-51	<5	17-25	7-35
Td	0.2-9.2	90-100	16-35	14-47	45-68	0.1-29	1.0-7.0	1.1-2.2	–0.03-2.1	2.2-3.6	17-32	29-44		13-25	5-32
Te	0.3-56	44-100	14-46	0.2-3	29-60	35-73	7.6-8.8	1.6-2.8	–0.5-0.1	2.0-4.8	40-60	25-30		22-46	<5
Homogeneous gravity flow (U)	0-47	52-100	17-35	2.4-7.7	29-44	51-65	8.0-8.6	2.0-2.8	–0.1-0.9	2.5-4.8	35-51	21-24	<5	22-40	<5-6
Contourite (MC)	0-32	68-100	23-36	14-35	37-55	30-48	7.0-7.5	2.2-2.8	–0.2- –0.5	2.5-2.9	29-39	16-26		<5	5-55
Debris flow (DF)	0-1.2	98-100	16-23	46-50	27-32	22-34	4.6-5.6	2.4-2.7	0.4-0.9	1.9-2.8	11-28	26-37	<5	15-26	19-56

Table 2. Correlation matrix of textural and bulk mineralogical data from Hole 976B.

	Biogenous	Terrigenous	$CaCO_3$	Sand	Silt	Clay	Grain size	Deviation	Skewness	Kurtosis	Phyllo-silicates	Quartz	Feldspar	Calcite	Dolomite
Biogenous	1.00														
Terrigenous	–1.00	1.00													
$CaCO_3$	0.36	–0.36	1.00												
Sand	–0.68	0.68	–0.43	1.00											
Silt	–0.35	0.35	–0.14	0.06	1.00										
Clay	0.74	–0.74	0.44	–0.92	–0.43	1.00									
Grain size	0.66	–0.66	0.43	–0.90	–0.39	0.96	1.00								
Deviation	–0.16	0.16	0.10	0.07	–0.28	0.04	0.21	1.00							
Skewness	–0.57	0.57	–0.57	0.74	0.48	–0.85	–0.87	–0.35	1.00						
Kurtosis	0.23	–0.23	0.44	–0.20	0.00	0.18	0.07	–0.23	–0.31	1.00					
Phyllosilicates	0.60	0.60	0.15	–0.83	–0.23	0.82	0.75	–0.16	–0.59	0.16	1.00				
Quartz	–0.65	0.65	–0.58	0.84	0.16	–0.83	–0.82	–0.04	0.72	–0.20	–0.78	1.00			
Feldspar	–0.13	0.13	–0.31	0.39	0.12	–0.45	–0.50	–0.28	0.38	0.15	–0.35	0.47	1.00		
Calcite	0.47	–0.47	0.65	–0.42	–0.31	0.51	0.45	0.15	–0.53	0.24	0.12	–0.40	–0.10	1.00	
Dolomite	–0.53	0.53	–0.03	0.55	0.25	–0.60	–0.47	0.09	0.44	–0.08	–0.57	0.26	–0.06	–0.60	1.00

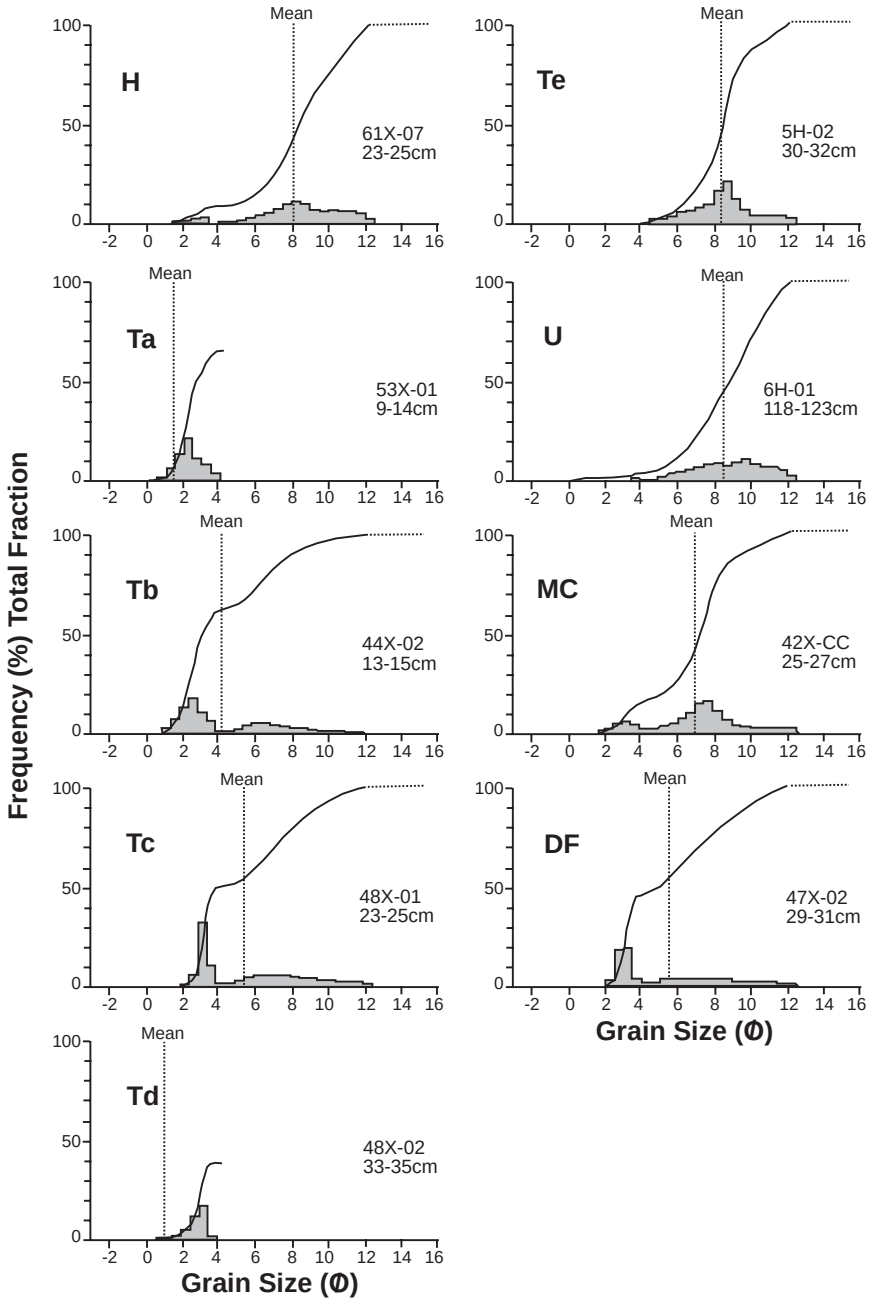

Figure 4. Textural cumulative curves and frequency histograms of sedimentary facies identified at Hole 976B. H = hemipelagic; Ta–Te correspond to the turbidite divisions of the Bouma sequence; U = homogeneous gravity flow; MC = muddy contourite; DF = debris flow.

sorted (2.6 ϕ–3.3 ϕ) silty sands (Fig. 6A) with a mean grain size of 4.4 ϕ and 5.0 ϕ. The total carbonate content ranges from 14% to 22%. The Td division corresponds to two textures: silty sand and muddy silt (Fig. 6B). The silty sand is moderately sorted sediment with a mean grain size of 1.1 ϕ (Fig. 4). The total carbonate content is high (27%–35%). The muddy silt is poorly sorted sediment with a mean grain size of 7.0 ϕ. The total carbonate content (< 20%) is lower than that of the silty sand. The Te division is characterized by moderate to poor sorting (1.6 ϕ–2.8 ϕ) with a mean grain size of 7.6 ϕ–8.8 ϕ (Fig. 4). These sediments have a mode at 8 ϕ–9 ϕ. The turbidite muds are ungraded and largely compose the Te3 structural division of Stow and Piper (1984). The Te division displays two types of mud (Fig. 6): one has a very low sand fraction content (<3%) of mostly terrigenous composition (60%–100%), and the other one is more sandy (≤8% of sand) with a mixed composition (~56% biogenous and 44% terrigenous components). In the first type, the carbonate content is low (<20%), whereas in the second type, it is higher (20%–46%).

Bulk-Mineralogical Characteristics

The bulk mineralogy of the turbidite facies exhibits a variable composition, which is related to the grain size (Fig. 7; Table 2). Table 2 shows that the grain size is correlated with the phyllosilicates (0.75) and calcite (0.45), and is inversely correlated with the quartz (–0.82), feldspar (–0.50), and dolomite (–0.47). Thus, the percentages of each mineralogical component of the turbidite facies are described on the

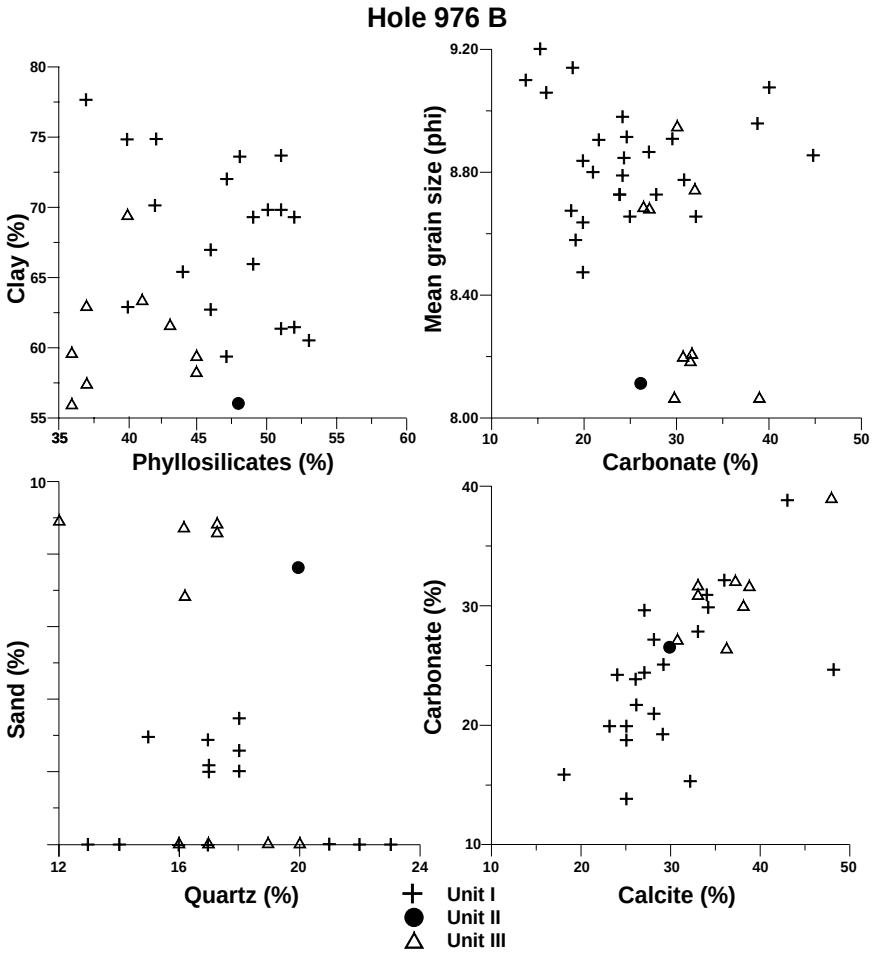

Figure 5. Binary plots showing some sedimentological (vertical axes) vs. mineralogical parameters (horizontal axes) of the hemipelagic sedimentary facies throughout lithostratigraphic Units I, II, and III from Hole 976B.

basis of grain-size distribution. The coarse grain size from the Ta to Tc divisions shows homogeneous composition. These divisions reveal the lowest values of phyllosilicates (5%–15%), whereas the Td division shows an increase in phyllosilicate percentages (17%–32%); their highest values correspond to the Te division (40%–60%). The behavior of quartz amounts in these turbidite divisions is opposite that of the phyllosilicates, as indicated by the correlation matrix (Table 2). Thus, the coarse grain size (Ta–Tc divisions) displays high quartz contents (≤63%), whereas the quartz content of the Td division ranges from 29% to 44%. The fine-grained sediment (Te division) contains low quartz percentages (25%–30%). The turbidite sediments contain low feldspar (<6%) and calcite (18%–25%) amounts, except for the Te division, which contains ≤46% calcite and a variable dolomite content (<5%–35%; Fig. 7; Table 1).

Homogeneous Gravity-Flow Facies

We identified homogeneous muds that are neither of obvious turbidite nor of settling origin. These muds are deposits of silty clay (29%–44% silt; 51%–55% clay) with a relatively high percentage of sand (3%–7%) in comparison with the turbidite muds. The homogeneous mud is very poorly sorted (2.0 ϕ–2.8 ϕ), with a mean grain size of 8.0 ϕ–8.6 ϕ (Fig. 4). The grain-size distribution is unimodal with a predominant mode in 9 ϕ. The sand fraction has a mixed composition (terrigenous 52%–100% and biogenous 0%–47% components). The total carbonate varies from 17% to 35%. The sediments are predominately dark greenish gray (5GY4/1) and minor layers are olive gray (5Y4/1) and grayish olive (10Y4/2). In general, this type of sediment is structureless, but a parallel lamination is defined by alternating grayish olive (10Y4/2) and grayish olive green (5GY3/2) in the interval 161-976B-35X, 25–27 cm (Shipboard Scientific Party, 1996). The different diagnostic features of the homogeneous muds indicate that these sediments were deposited by gravity flows, rather than by settling from suspension (pelagic or hemipelagic), according to the depositional model proposed by Stanley (1981) to explain the origin of unifites in Mediterranean basins (Alboran Basin, Hellenic Trench, and Corsican Trench). Stanley (1981) suggested the term “unifites” and considered them as the end-products of sediment gravity flows, which are probably related to mud-charged turbidity currents and are less dense than turbid-layer flows. Before the definition of unifites, the muds in the Alboran Sea were attributed to transport of largely terrigenous clay-size particles basinward by low-density, gravity-assisted currents (Stanley et al., 1970; Huang and Stanley, 1972).

Bulk-Mineralogical Characteristics

The homogeneous gravity-flow facies exhibit relatively high contents of phyllosilicate (35%–51%) and calcite (22%–40%), with relatively low amounts of quartz (21%–24%) and dolomite (<5%–6%). The bulk-mineralogical characteristics of this facies show significant similarities with those described in the hemipelagic facies (H2 type) and turbidite mud (Table 1).

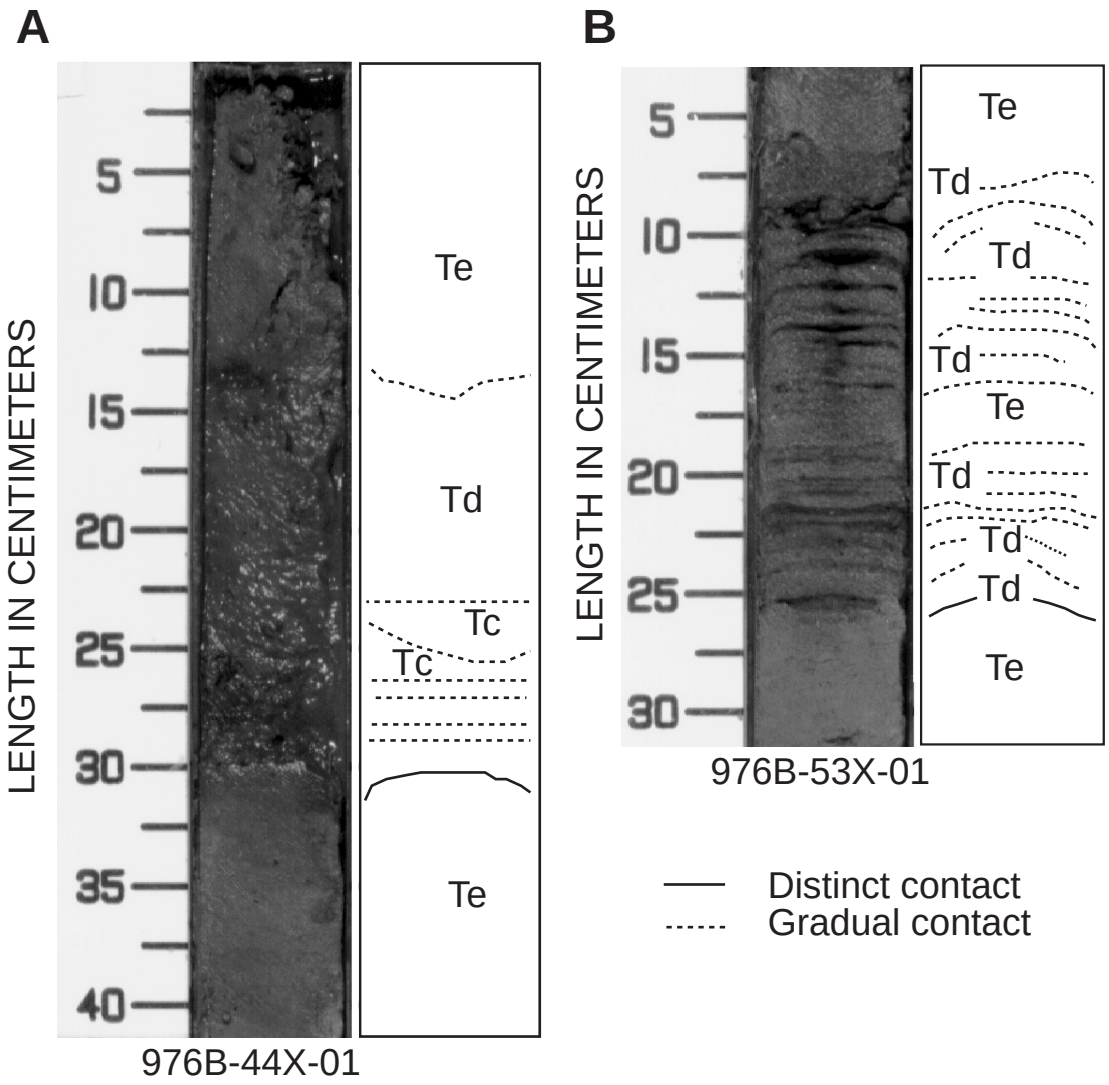

Figure 6. Some of the most characteristic turbidite associations: **(A)** clay, sand, silt, clay; and **(B)** clay, silt, clay lithologies. Tb, Tc, Td, Te refer to the different divisions of the Bouma sequence already indicated in Figure 4.

Contourite Facies

Sedimentological Characteristics

Despite the difficulty in separating turbidite from contourite deposits, especially when bottom currents modify deposits containing turbidites (Faugères and Stow, 1993), we identified muddy contourites in Hole 976B. These contourite sediments are differentiated from turbidite muds on the basis of the following diagnostic parameters: (a) the bimodal grain-size distribution, (b) poor preservation of foraminifers, (c) the lack of vertical grading of sedimentary structures, (d) the very poor sorting, (e) the relatively high percentage of sand (≤14.8%), and (f) the mixed nature of the sand fraction. The muddy contourites are represented in only two samples (161-976B-39X-5, 90–95 cm; 42X-CC, 25–27 cm), which correspond to silty clays and clayey silts and are characterized by very poor sorting (2.2 ϕ–2.8 ϕ) and a mean grain size (7.0–7.5 ϕ) lower than that of the turbidite mud (Fig. 4; Table 1). The total carbonate content is relatively high (23%–36%). The sediments are olive gray (5Y4/1) and dark green gray (5GY4/1).

Bulk-Mineralogical Characteristics

The bulk mineralogy of the contourite facies contains a relatively low content of phyllosilicates (29%–39%) and quartz (16%–26%), a very low content of calcite (< 5%), and a variable dolomite content (5%–55%) (Table 1).

Debris-Flow Facies

Several layers from Hole 976B are interpreted as deposits resulting from debris flows. This type of sediment is differentiated on the basis of the degree of internal deformation. The debris-flow sediments correspond to sandy sediments (sandy silts and silty sands), with a high percentage of clay (22%–34%) that contrasts with classical sand-silt turbidites. This sediment is very poorly sorted (2.4 ϕ–2.7 ϕ), and has a median grain size of 4.6 ϕ–5.6 ϕ (Fig. 4; Table 1). Figure 8 shows a disorganized structure at interval 161-976B-43X-1, 60–100 cm, with mud balls (≤3 cm wide) and irregular pockets, and a darker (coarser sediment) or lighter (finer sediment) color. A sharp basal contact is identified in some layers (e.g., 161-976B-48X-1, 23–

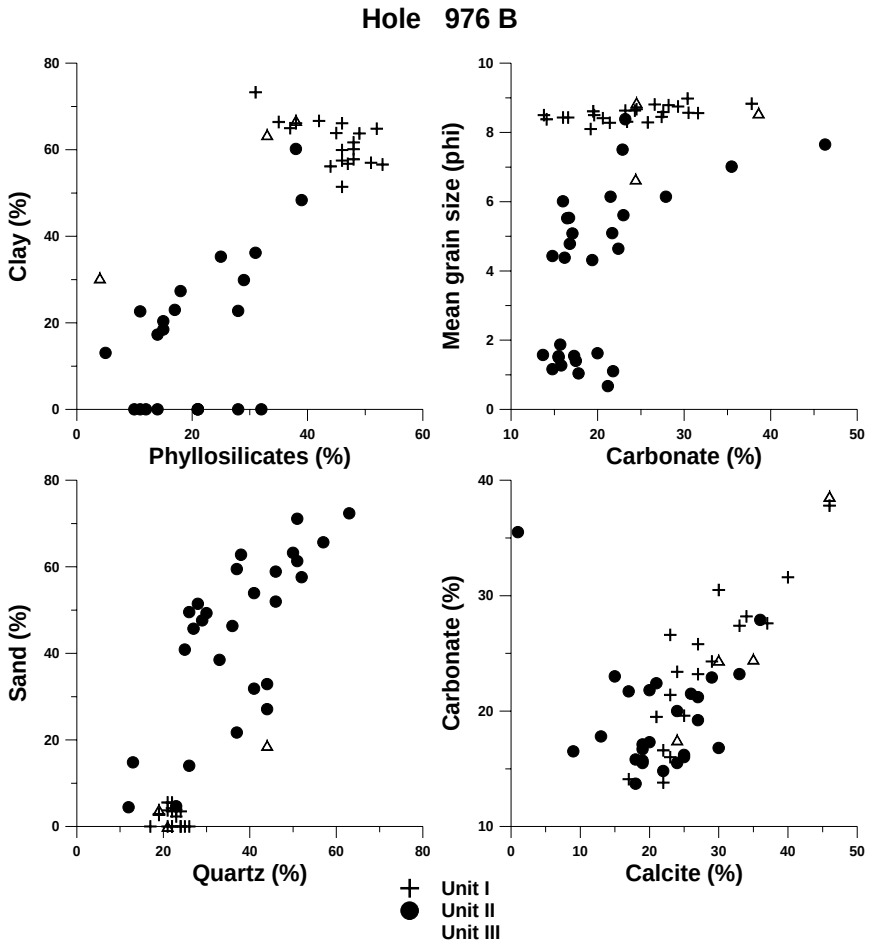

Figure 7. Binary plots showing some sedimentological (vertical axes) vs. mineralogical parameters (horizontal axes) of the turbidite sedimentary facies throughout lithostratigraphic Units I, II, and III from Hole 976B.

25 cm). The total carbonate content varies from 16% to 23%. The sediments are dark (medium dark gray, N4; dark gray, N3; and olive gray, 5Y4/1).

Bulk-Mineralogical Characteristics

The bulk mineralogy of the debris-flow facies consists of low amounts of phyllosilicates (11%–28%), quartz (26%–37%), feldspar (<5%), and calcite (15%–26%), with variable dolomite contents (19%–56%; Table 1).

DISCUSSION

Sediment Sources

Two sources for the sediments could be established: (1) a biogenic input of hemipelagic facies, and (2) a terrigenous input from the margin, mainly through the Fuengirola Canyon. This terrigenous source is suggested first by the proximity of Site 976 to Fuengirola Canyon (Fig. 1). The high-resolution seismic profile shown in Figure 3 illustrates the sedimentary facies near Site 976. These seismic facies reflect the development of different channel-levee complexes within the upper Pliocene seismic unit, which is correlated to lithostratigraphic Unit II. The existence of these turbidite elements (channel-levee complexes) therefore corroborates the origin of the successions of turbidite sequences (Ta–Te) defined in Unit II, from late Pliocene to early Pleistocene. Thus, the large amount of coarse-terrigenous sediments could have been transported into the head of the Fuengirola Canyon and subsequently funneled basinward. The relatively uniform bulk-mineral composition of hemipelagic and turbidites suggests a common source area for the two sediment types. However, the significant increase in dolomite in Unit II also supports a source for this mineral on land.

Facies Associations and Their Evolution in Time

Six facies associations from A to F can be recognized on the basis of the thickness and vertical distribution of the different sedimentary facies described above. The type A facies association is composed, from base to top, of turbidite mud (Te), homogenous gravity-flow mud (U), and hemipelagic mud (H). The thickness of the different sedimentary facies ranges from 1 to 10 m. This facies association has developed only in lithostratigraphic Unit I and is present only in its uppermost section (0–223 mbsf). The type B facies association is defined by turbidite mud (Te) that changes upward to homogeneous gravity-flow mud (U); its thickness varies from 5 to 8 m. This facies association occurs in the uppermost section of Unit I (0–223 mbsf) and intercalates with the type A facies association.

The type C facies association consists of an alternation of turbidite mud (Te) and hemipelagic mud (H) with variable bed thicknesses,

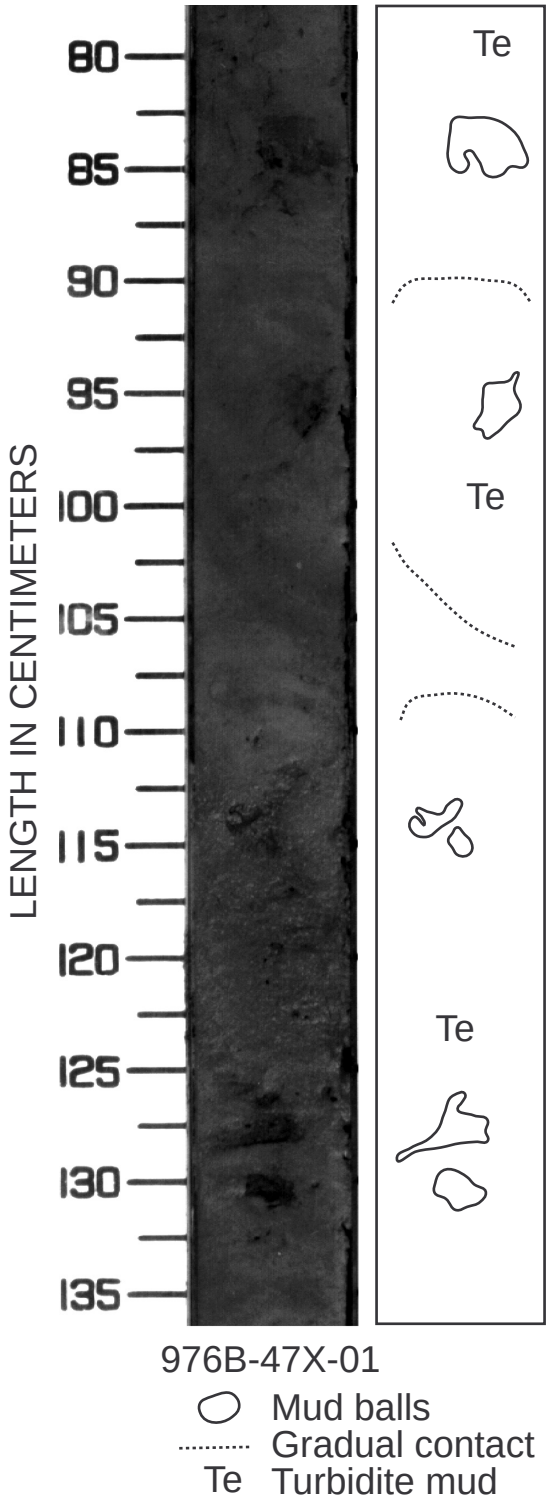

Figure 8. Debris-flow facies showing the disorganized character with mud balls at Hole 976B. Te = turbidite mud.

from 2 to 30 m. The facies is identified in the lower section of lithostratigraphic Unit I (223–362 m depth, mbsf) and Unit III (518–573 m depth, mbsf). The type D facies association contains alternating turbidite sand, silt, and mud, and only occurs in lithostratigraphic Unit II. The base of this turbidite association is generally defined by a sharp boundary (Fig. 6). The Ta–Tb intervals are present, although the most frequent intervals are represented by Tc-Td and Td-Te. The type E facies association is composed of debris-flow sediments (DF) overlying the type D facies association (mostly formed of the Td division). This association is rarely in Unit II (e.g., Samples 161-976B-47X-2, 29–31 cm, 47X-2, 33–35 cm, 47X-CC, 2–4 cm, 48X-1, 23–25 cm). A similar distribution pattern occurs with the type F facies association, defined by muddy contourites (MC), which occurs at the top of Unit II (e.g., 161-976B-39X-5, 90–95 cm, and 42X-CC, 28–30 cm).

The general distribution of facies association types throughout the three lithostratigraphic Units I–III corresponding to the Pliocene and Pleistocene section in Hole 976B is shown in Figure 9. Facies association A accounts for ~27% of the stratigraphic section of Unit I of Pleistocene age. Facies association B represents 16% of Unit I, although it is absent from all other units. In contrast to these associations, facies association C is the most significant in the composition of Unit I (~57%) and Unit III (100%), of Pleistocene and early Pliocene age, respectively. Facies association D accounts for ~98% of Unit II of lower Pleistocene and upper Pliocene age. Facies association E (DF) and F (MC) represent only 1% of Unit II (Fig. 9).

Pliocene and Pleistocene Depositional History

The Pliocene and Pleistocene depositional history at the base-of-slope of the Málaga margin in the northwestern Alboran Sea is governed by the occurrence of five major sedimentary processes responsible for the deposition of facies identified in Hole 976B: (1) normal, pelagic settling of terrigenous particles introduced by rivers and wind, and of marine microskeletons (hemipelagic facies); (2) turbidity currents transporting dominantly terrigenous sediments from shallower environments onto the base-of-slope (turbidite facies); (3) low-density gravity flows related to episodic, but frequent, failure of sediment and an associated successions of downslope, redepositional events that led to unifite deposition (homogeneous gravity-flow facies); (4) bottom currents; and (5) debris flows involving gravity-driven movements of mixtures of sediment particles and water (debris-flow facies). Processes 3 and 5 may have been favored during falling and lowstand sea levels and by catastrophic events such as slope failure, triggered by earthquakes or slope oversteepening. This idea is supported by geotechnical evidence, at least for the most recent sediments (late Pleistocene/Holocene; Baraza et al., 1992). The western Alboran slope can be characterized as potentially unstable on the basis of physical properties of sediments and knowledge of the seismicity of the area (Sanz de Galdeano and López Casado, 1988; Baraza et al., 1992).

The sedimentological and mineralogical data of the northwestern Alboran Basin allow us to establish three sedimentary stages to explain the Pliocene and Pleistocene depositional evolution of this area according to the dominant sedimentary sequences: Stage I (early Pliocene: hemipelagic settling and turbidite currents of low energy); Stage II (early Pleistocene/late Pliocene: turbidite currents, bottom currents, and debris flows); and Stage III (Pleistocene: hemipelagic settling and gravity flows of low energy) (Fig. 10). Stage I could correspond to the flooding of the Mediterranean Sea through the Strait of Gibraltar and the generalized global high sea level during the early Pliocene (Alonso and Maldonado, 1992; Estrada et al., in press). This stage resulted predominantly in hemipelagic sedimentation with few mud turbidite layers forming the facies association C (Te–H; Fig. 10). After this time, during Stage II, a generalized and pronounced sea-level lowering occurred during the late Pliocene (Vail et al., 1977), which favored the development of the Fuengirola turbidite system, as revealed by the seismic facies and lithologic composition of the turbidite sediments (Figs. 3, 10). Contourite and debris-flow facies were deposited during this stage, but in lower percentages. The sedimentary facies deposited during Stage III corresponds to the Pleistocene, when high-frequency and high-amplitude sea-level changes occurred (Ercilla and Alonso, 1996; Estrada et al., in press). The prevailing sediments deposited during this stage are fine grained

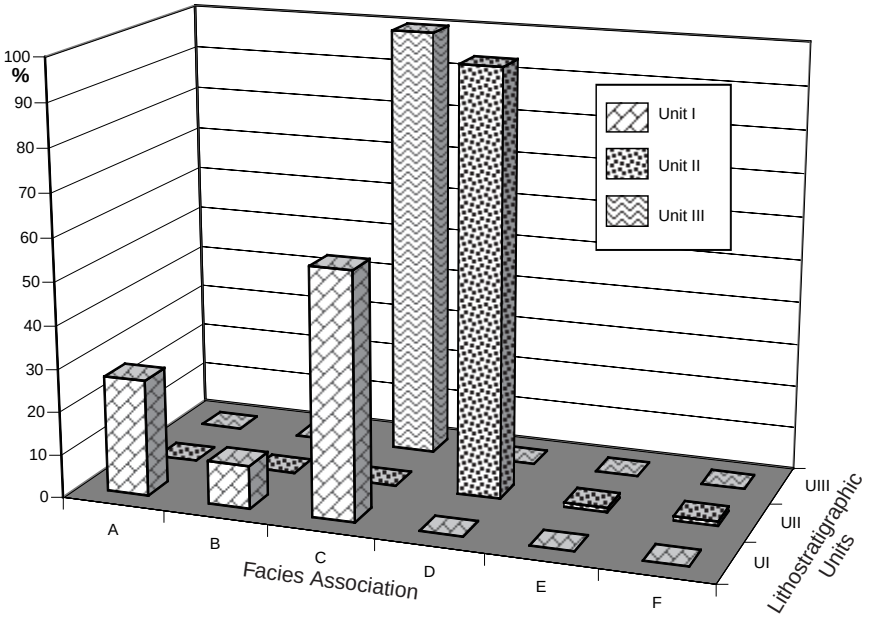

Figure 9. Quantification (0–100%) of facies association types (A–F) throughout lithostratigraphic Units I, II, and III from Hole 976B. Flat symbols represent zero. See explanation in the text.

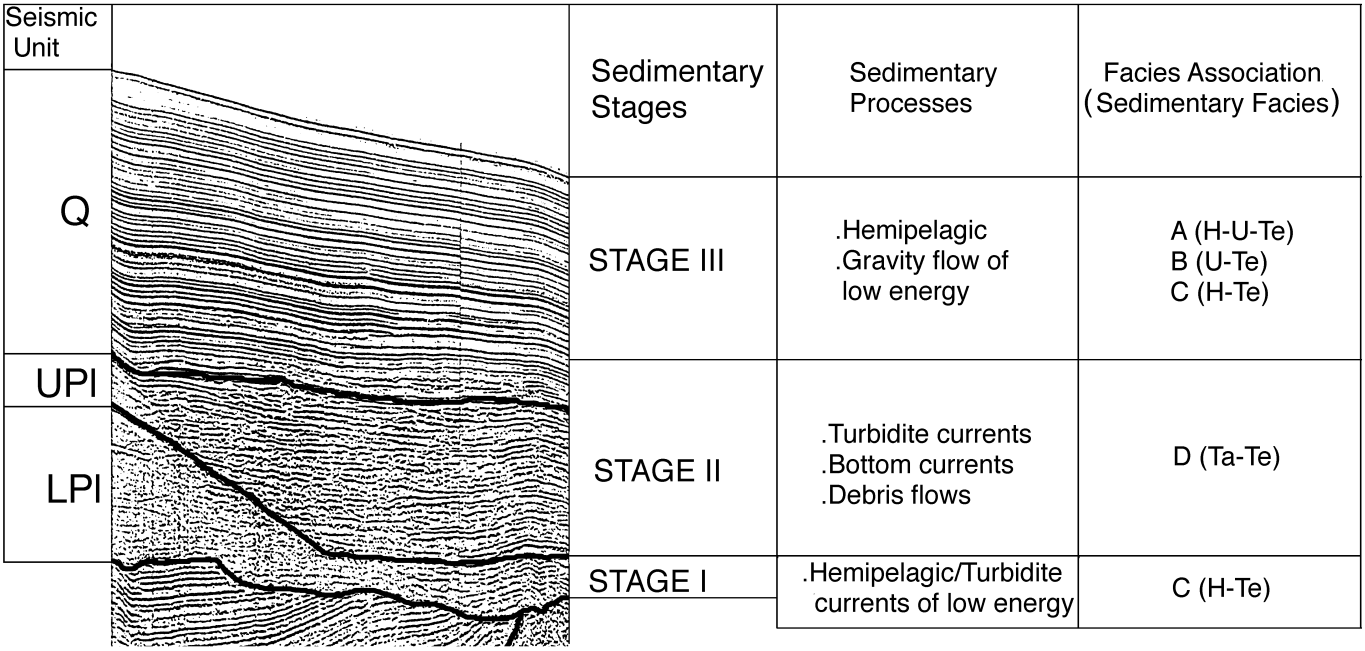

Figure 10. Pliocene and Pleistocene depositional history in the northwestern Alboran Sea showing the Pliocene–Quaternary seismic units. The distribution of facies association (A–C) <15% throughout the Pliocene and Pleistocene section are not indicated. Q = Quaternary seismic unit; UPl = upper Pliocene seismic unit; LPl = lower Pliocene seismic unit (see explanations in text). Letters for facies associations and sedimentary facies are explained in Figure 2; seismic line corresponds to that in Figure 3.

and include both hemipelagic and gravity flows of low energy, as revealed by the presence of fine-grained facies associations A (Te–U–H), B (Te–U), and C (Te–H) (Fig. 10).

ACKNOWLEDGMENTS

We greatly appreciate the assistance of the Shipboard Scientific Party and the crew of the *JOIDES Resolution* in the acquisition of these samples. We thank N. Maestro and B. Paracuellos for their help in the laboratory. J.M. Anguita drew the final figures. This work was supported through the "C.I.C.Y.T." of Spain under grant AMB-95-0196 (B.A., G.E., J.B., and A.G.) and AMB-95-1557 (F.M.-R.).

REFERENCES

Alonso, B., and Maldonado, A., 1990. Late Quaternary sedimentation of the Ebro turbidite systems (Northwestern Mediterranean): two styles of deep-sea deposition. *Mar. Geol.*, 95:353–377.

————, 1992. Plio-Quaternary margin growth patterns in a complex tectonic setting: northeastern Alboran Sea. *Geo-Mar. Lett.,* 12:137–143.

Baraza, J., Ercilla, G., and Lee, H.J., 1992. Geotechnical properties and preliminary assessment of sediment stability on the continental slope of the northwestern Alboran Sea. *Geo-Mar. Lett.,* 12:150–156.

Bates, R.L., and Jackson, J.A. (Eds.), 1987. *Glossary of Geology* (3rd ed.): Alexandria, VA (Am. Geol. Inst.).

Comas, M.C., García-Dueñas, V., and Jurado, M.J., 1992. Neogene tectonic evolution of the Alboran Basin from MCS data. *Geo-Mar. Lett.,* 12:157–164.

Dewey, J.F., Helman, M.L., Turco, E., Hutton, D.H.W., and Knott, S.D., 1989. Kinematics of the western Mediterranean. *In* Coward, M.P., Dietrich, D., and Park, R.G. (Eds.), *Conference on Alpine Tectonics.* Geol. Soc. Spec. Publ. London, 45:265–283.

Dillon, W.P., Robb, J.M., Greene, H.G., and Lucena, J.C., 1980. Evolution of the continental margin of Southern Spain and the Alboran Sea. *Mar. Geol.,* 36:205-226.

Ercilla, G., and Alonso, B., 1996. Quaternary siliciclastic sequence stratigraphy of western Mediterranean passive and tectonically active regions: the role of global versus controlling factors. *In* De Batist, M., and Jacobs, P. (Eds.), *Geology of Siliciclastic Shelf Seas.* Geol. Soc. Spec. Publ. London, 117:125–137.

Ercilla, G., Alonso, B., and Baraza, J., 1992. Sedimentary evolution of the northwestern Alboran Sea during the Quaternary. *Geo-Mar. Lett.*, 12:144–149.

————, 1994. Post-Calabrian sequence stratigraphy of the northwestern Alboran Sea (Southwestern Mediterranean). *Mar. Geol.,* 120:249–265.

Estrada, F., Ercilla, G., and Alonso, B., in press. Pliocene-Quaternary tectosedimentary evolution of the NE Alboran Sea (SW Mediterranean Sea). *In* Cloetingh, E., and Fernandez, M. (Eds.). *Origin of Sedimentary Basins.* Tectonophysics, Spec. Vol.

Faugères, J.-C., and Stow, D.A.V., 1993. Bottom-current-controlled sedimentation: a synthesis of the contourite problem. *Sediment. Geol.,* 82:287–297.

Forrest, J., and Clark, N.R., 1989. Characterizing grain size distributions: evaluation of a new approach using a multivariate extension of entropy analysis. *Sedimentology,* 36:711–722.

Friedman, G.M., and Sanders, J., 1978. *Principles of Sedimentology:* New York (Wiley), 58–81.

Giró, S., and Maldonado, A., 1985. Análisis granulométrico por métodos automáticos: tubo de sedimentación y Sedigraph. *Acta Geol. Hisp.*, 20:95–102.

Hesse, R., and Butt, A., 1976. Paleobathymetry of Cretaceous turbidite basins of the East Alps relative to the calcite compensation level. *J. Geol.*, 84:505–533.

Huang, T.-C., and Stanley, D.J., 1972. Western Alboran Sea: sediment dispersal, ponding and reversal of currents. *In* Stanley, D.J. (Ed.), *The Mediterranean Sea: a Natural Sedimentation Laboratory:* Stroudsburg, PA (Dowden, Hutchinson, and Ross), 521–559.

Jurado, M.J., and Comas, M.C., 1992. Well log interpretation and seismic character of the Cenozoic sequence in the Northern Alboran Sea. *Geo-Mar. Lett.,* 12:129–136.

Krenmayr, H.G., 1996. Hemipelagic and turbiditic mudstone facies associations in the Upper Cretaceous Gosau group of the Northern calcareous Alps (Austria). *Sediment. Geol.,* 101:149–172.

Maldonado, A., Campillo, A.C., Mauffret, A., Alonso, B., Woodside, J., and Campos, J., 1992. Alboran Sea late Cenozoic tectonic and stratigraphic evolution. *Geo-Mar. Lett.,* 12:179–186.

Porebski, S.J., Meischner, D., and Gorlich, K., 1991. Quaternary mud turbidites from the South Shetland Trench (West Antarctica): recognition and implications for turbidite facies modelling. *Sedimentology,* 38:691–715.

Rupke, N.A., and Stanley, D.J., 1974. Distinctive properties of turbiditic and hemipelagic mud layers in the Algero-Balearic Basin Western Mediterranean Sea. *Contrib. Earth Sci.,* 13:1–40.

Sanz de Galdeano, C., and López Casado, C., 1988. Fuentes sísmicas en el ámbito bético-rifeño. *Rev. Geof.,* 44:175–198.

Shipboard Scientific Party, 1973. Western Alboran Basin Site 121. *In* Ryan, W.B.F., Hsü, K.J., et al., *Init. Repts. DSDP,* 13: Washington (U.S. Govt. Printing Office), 43–89.

————, 1996. Site 976. *In* Comas, M.C., Zahn, R., Klaus, A., et al., *Proc. ODP, Init. Repts.,* 161: College Station, TX (Ocean Drilling Program), 179–297.

Stanley, D.J., 1981. Unifites: structureless muds of gravity-flow origin in Mediterranean basis. *Geo-Mar. Lett.,* 1:77–84.

Stanley, D.J., Gehin, C.E., and Bartolini, C., 1970. Flysch-type sedimentation in the Alboran Sea, Western Mediterranean. *Nature,* 228:979–983.

Stow, D.A.V., 1994. Deep sea processes of sediment transport and deposition. *In* Pye, K. (Ed.), *Sediment Transport and Depositional Processes:* London (Blackwell), 257–291.

Stow, D.A.V., and Faugères, J.C. (Eds.), 1993. *Contourites and Bottom Currents.* Sediment. Geol., Spec. Vol., 82:1–310.

Stow, D.A.V., and Piper, D.J.W., 1984. Deep-water fine-grained sediments: facies models. *In* Stow, D.A.V., and Piper, D.J.W. (Eds.), *Fine-Grained Sediments: Deep-Water Processes and Facies.* Geol. Soc. Spec. Publ. London, 15:611–645.

Swan, D., Clague, J.J., and Luternauer, J.L., 1979. Grain-size statistics II: evaluation of grouped moment measures. *J. Sediment. Petrol.,* 94:487–500.

Vail, P.R., Mitchum, R.M., Jr., and Thompson, S., III, 1977. Seismic stratigraphy and global changes of sea level, Part 4. Global cycles of relative changes of sea level. *In* Payton, C.E. (Ed.), *Seismic Stratigraphy: Applications to Hydrocarbon Exploration.* AAPG Mem., 26:83–97.

Vatan, A., 1967. *Manuel de Sédimentologie:* Paris (Technip.).

Watts, A.B., Platt, J.P., and Bulh, P., 1993. Tectonic evolution of the Alboran Sea Basin. *Basin Res.,* 5:153–177.

Date of initial receipt: 7 May 1997
Date of acceptance: 21 January 1998
Ms 161SR-206